Published in final edited form as:
Nucl Med Biol. 2008 April ; 35(3): 287–298. doi:10.1016/j.nucmedbio.2008.01.001.

Comparison of the Pharmacokinetics of Different Analogs of ^{11}C-Labeled TZTP for Imaging Muscarinic M2 Receptors with PET

Alicia E. Reid[1], **Yu-Shin Ding**[2], **William C. Eckelman**[3], **Jean Logan**[1], **David Alexoff**[1], **Colleen Shea**[1], **Youwen Xu**[1], and **Joanna S. Fowler**[1]

[1]Brookhaven National Laboratory, Upton, NY, USA 11973

[2]Radiology Department, Yale University School of Medicine, New Haven, CT, USA

[3]Molecular Tracer LLC, Bethesda, Maryland, USA 20892

Abstract

Introduction—The only radiotracer available for the selective imaging of muscarinic M2 receptors in vivo is 3-(3-{3-[^{18}F]fluoropropyl)thio}-1,2,5-thiadiazol-4-yl)-1,2,5,6-tetrahydro-1-methylpyridine) ([^{18}F]FP-TZTP). We have prepared and labeled FP-TZTP and two other TZTP derivatives with ^{11}C at the methylpyridine moiety to explore the potential of using C-11 labeled FP-TZTP for PET imaging of M2 receptors and to compare the effect of small structural changes on tracer pharmacokinetics (PK) in brain and peripheral organs.

Methods—^{11}C radiolabeled [FP-TZTP, **3**], 3-(3-propyl)-TZTP [P-TZTP, **6**], 3,3,3-(3-(3-trifluoropropyl)-TZTP [F_3P-TZTP, **10**] were prepared and log D, plasma protein binding (PPB), affinity constants, time-activity curves (TACs), area under the curve (AUC) for arterial plasma, distribution volumes (DV) and pharmacological blockade in baboons were compared.

Results—Values for log D, PPB and affinity constants were similar for **3**, **6** and **10**. The fraction of parent radiotracer in the plasma was higher and the AUC lower for **10** than for **3** and **6**. TACs for brain regions were similar for **3** and **6**, which showed PK similar to the F-18 tracer, while **10** showed slower uptake and little clearance over 90 min. DV's for **3** and **6** were similar to the F-18 tracer but higher for **10**. Uptake of the three tracers was significantly reduced by coinjection of unlabeled **3** and **6**.

Conclusion—Small structural variations on the TZTP structure greatly altered the PK in brain and behavior in blood with little change in the log D, PPB or affinity. The study suggests that ^{11}C radiolabeled **3** will be a suitable alternative to [^{18}F]FP-TZTP for translational studies in humans.

Keywords

PET; muscarinic M2; pharmacokinetics; TZTP; carbon-11

Corresponding Author: Alicia Reid, Medical Department, Bldg555, Brookhaven National Laboratory, Upton, NY, 631-344-4393 (phone), 631-344-5815 (fax), areid@bnl.gov.

1 Introduction

Interest in radioligands for the selective imaging of the muscarinic M2 receptor in vivo was sparked by Quirion and Aubert's observation of a loss of this subtype in the cortex of Alzheimer's patients [1–3]. Measurements of muscarinic M2 receptors could also serve as a surrogate measure of the cholinergic pathway as these receptors are primarily located presynaptically on cholinergic neurons. Relative to other muscarinic subtypes in the central nervous system (CNS) M2 receptors are in low concentration. This necessitates that a potential radioligand possess high affinity and selectivity. In addition to being in low concentration, M2 receptors are distributed relatively uniform in the brain gray matter and no clear receptor free region that can be used as a reference region has been identified [4–5]. Kinetic modeling of imaging data is therefore crucial to obtain quantitative information about binding site availability. Together with suitable kinetics that allows modeling of the data and high in vivo selectivity and affinity, potential radioligands for M2 receptors must also meet the general requirements for PET radiotracers for the CNS. Criteria for PET radiotracers for the CNS include slow metabolism of the tracer in the brain, low brain permeation of systemic metabolites and those requirements outlined by Lipinski's rules for blood brain barrier (BBB) penetration [6].

Several 3-(3-substituted-1,2,5-thiadiazol-4-yl)-1,2,5,6-tetrahydro-1-methylpyridines) (substituted TZTPs) have been investigated for the selective imaging of muscarinic receptors in vivo. The subtype selectivity and agonist/antagonist characteristics of these derivatives depend on the chain length of the alkyl side chain [7]. Iodinated TZTP derivatives for imaging M2 receptors with single photon emission computed tomography (SPET), for example, failed to demonstrate specific binding in vivo [8]. For positron emission tomography (PET) imaging the [^{18}F]fluoroethylthio TZTP derivative failed to show specific binding to M2 receptors in vivo [9] and the [^{11}C]butylthio TZTP derivative, an M1 agonist radiotracer was shown to be unsuitable because of its high affinity for sigma-1 receptors [10].

Recently 3-(3-{3-[^{18}F]fluoropropyl)thio}-1,2,5-thiadiazol-4-yl)-1,2,5,6-tetrahydro-1-methylpyridine) ([^{18}F]FP-TZTP) was introduced as a M2 selective agonist radiotracer for PET imaging of M2 receptors in vivo [11–12]. [^{18}F]FP-TZTP was shown to exhibit modest in vitro selectivity for M2 (2.2nM) over M1 (7.4nM) and low affinity for all other biogenic amine systems [12]. The in vivo selectivity of this radiotracer for the M2 subtype was demonstrated by coinjection with the M2 selective agonist propylthio-TZTP and confirmed in experiments using gene-manipulated, knockout (KO) mice [13–14]. The sensitivity of [^{18}F]FP-TZTP binding to endogenous acetylcholine concentration has been established by a competition model after treatment with the cholinesterase inhibitor physostigmine [11]. The correlation between [^{18}F]FP-TZTP binding and the two main risk factors for AD, age and the inheritance of the ε4 allele, have been investigated [15–16]. An increase in [^{18}F]FP-TZTP binding was observed in APOE-ε4+ subject versus APOE-ε4- controls and in cognitively normal older subjects versus younger subjects. The results were attributed to a decrease in acetylcholine in the synapse of the APOE-ε4+ and older subjects as compared to APOE-ε4- and younger controls respectively. [^{18}F]FP-TZTP was therefore proposed for use in making in vivo measurements of muscarinic systems biology rather than M2 receptor density alone. Reduction in M2 receptor binding in bipolar disorder subjects relative to healthy controls and subjects with major depressive disorder was demonstrated using [^{18}F]FP-TZTP binding studies [17]. [^{18}F]FP-TZTP has also been used to study the mechanism underlying the effect of procaine on mood and emotion [18].

P-TZTP was reported by Sauerberg to possess higher in vitro selectivity than FP-TZTP, for M2 receptors, but this compound was not labeled and studied in vivo [12]. No reports were found in the literature for the synthesis or study of F_3P-TZTP.

[^{18}F]FP-TZTP remains the only probe available for imaging M2 receptors in vivo with PET. Since the FP-TZTP molecule contains an N-methyl group and since the brain kinetics of the F-18 derivative are relatively rapid, we set out to label FP-TZTP with carbon-11, which allows multiple PET studies at 2 h time intervals. We also synthesized two other precursors with small changes in the S-alkyl group to compare the effect of small structural changes on physico-chemical properties and pharmacokinetics in the baboon. We prepared ^{11}C radiolabeled 3-(3-(3-fluoropropylthio)-1,2,5-thiadiazol-4-yl)-1,2,5,6-tetrahydro-1-methylpyridne [FP-TZTP, **3**], 3-(3-propylthio)-TZTP [P-TZTP, **6**], 3,3,3-(3-(3-trifluoropropylthio)-TZTP [F_3P-TZTP, **10**] and compared log D, free fraction in plasma, affinity for M1 and M2 muscarinic receptors, time-activity curves (TACs) in brain and peripheral organs, area under the curve (AUC) for arterial plasma, distribution volumes (DV) and pharmacological blockade in baboons.

2 Methods

2.1 Materials

All reagents and solvents were purchased from commercial suppliers. When necessary solvents were further purified or dried according to procedures outlined in Purification of Laboratory Chemicals [19]. Melting points are uncorrected and were performed on a Fisher-Johns melting point apparatus. NMR spectra were determined using a Bruker Avance 400MHz NMR spectrrometer (400 MHZ for ^{1}H and 100 MHz for ^{13}C) and referenced to the NMR solvent used. $^{11}CO_2$ produced by BNL's EBCO cyclotron via the $^{14}N(p,\alpha)^{11}C$ nuclear reaction using 100ppm O_2 in N_2 as the target gas, was converted to $^{11}CH_4$ by Ni catalyzed hydrogenation and reaction with I_2 in an automated GE PET trace MeI Microlab (GE Medical Systems, Milwaukee, WI) gave no-carrier added $^{11}CH_3I$. Radioactivity measurements were made in a Capintec CRC-712MV radioisotope calibrator (Capintec Inc., Ramsey, NJ) and small radioactive samples were measured in a Packard MINAXI γ 5000 automated gamma counter. Semipreparative HPLC was performed using a Knauer HPLC system equipped with a model K-1001 pump, a model 87 variable wavelength monitor, a NaI radioactivity detector, a Hewlet Packard 3390A integrator, and a SRI Peak Simple Integration System. Analytical HPLC was performed using a Knauer model K-1001 pump, a Knauer model K2501 UV detector (254nm), a NaI radioactivity detector and two Hewlett Packard 3390A integrators. For thin layer chromatography (TLC) analyses of radiotracers, Macherey-Nagel (MN) polygram sil G/UV254 plastic-back TLC plates and a Bioscan System 200 imaging scanner were used.

2.2 Chemical Syntheses

Compounds **1**, **4** and **7** were prepared, in multiple steps, according to literature procedures [7,12,20,21]. Demethylation of **1**, **4** and **8** gave the corresponding desmethyl precursor compounds for radiolabeling, as shown in Figure 2.

2.2.1 3-(3-(3-Fluoropropylthio)-1,2,5-thiadiazol-4-yl)-1,2,5,6-tetrahydropyridine (2)—To a solution of **1** (0.059 g, 0.22 mmol) in dry dichloroethane (DCE) (1.5 ml) was added vinyl chloroformate (0.03 ml, 0.33 mmol) and the resulting mixture heated under reflux for 2 h. The mixture was cooled to rt, water (5 ml) and conc. HCl (0.2 ml) were added and the resulting mixture extracted with Et_2O (3 × 10 ml). The combined ether extract was concentrated and the residue heated under reflux with methanolic HCl for 2 h. The solvent was then evaporated and the residue crystallized from MeOH/Et_2O to give the HCl salt of **2**

as a pale brown solid (0.035 g, *yield = 63%*): ^{1}H NMR (MeOD) δ: 6.96 (1H, m), 4.55 (1H, m), 4.44 (1H, m), 4.14 (2H, d, J = 2Hz), 3.39 (4H, m), 2.66 (2H, m), 2.12 (2H, m).

^{13}C NMR (MeOD) δ: 157.26, 155.81, 130.32, 126.25, [84.27, 82.63], 43.96, 41.23, [31.42, 31.22], [30.06, 30.00]. Compound **2** was obtained as the free base (pale brown oil) by an aqueous sodium carbonate wash. HPLC analysis showed trace contamination by **1** and the product was further purified by column chromatography on silica gel using gradient elution: hexane to hexane/EtOAc (50/50) as the eluent. Compound **2** was obtained as a brown oil (0.022 g, 39%) ^{1}H NMR (MeOD) δ: 6.74 (1H, m), 4.54 (1H, m), 4.43 (1H, m), 3.68 (2H, d, J = 2Hz), 3.27 (2H, m), 2.90 (2H, m), 2.30 (2H, m), 2.09 (2H, m). ^{13}C NMR (MeOD) δ: 158.21, 157.03, 131.86, 131.66, [84.32, 82.68], 46.74, 42.78, [31.48, 31.28], [29.91, 29.86], 26.22.

2.2.2 3-(3-Propylthio)-1,2,5-thiadiazol-4-yl)-1,2,5,6-tetrahydropyridine (5)—To a solution of **4** (0.83 g, 3.25 mmol) in DCE (6 ml) was added vinyl chloroformate (0.45 ml, 4.93 mmol) and the resulting mixture heated under reflux for 2 h. After heating at reflux for 2 h the mixture was cooled to rt, water (6 ml) and conc. HCl (2 ml) were added and the mixture extracted with Et_2O (4 × 20 ml). The combined ether extract was concentrated then heated under reflux with methanolic HCl for 2 h. The solvent was then evaporated and the residue crystallized from MeOH/Et_2O to give the HCl salt of **5** as a pale brown solid (0.264 g, *yield = 29%*): ^{1}H NMR (MeOD) δ: 7.04 (1H, s_{br}), 4.20 (2H, s_{br}), 3.43 (2H, s_{br}), 3.33 (2H, m), 2.73 (2H, s_{br}), 1.81 (2H, M), 1.06 (3H, t, J = 7.2). Compound **5** was obtained as the free base (brown oil, 0.206 g) by an aqueous sodium carbonate wash. HPLC analysis showed trace contamination by **4** and the product was further purified by column chromatography on silica gel using gradient elution: hexane to hexane/EtOAc (50/50) as the eluent. Compound **5** was obtained as a brown oil (0.140 g, 18%):^{1}H NMR ($CDCl_3$) δ: 6.77 (1H, m), 3.81 (2H, s_{br}), 3.24 (2H, m), 3.03 (2H, m), 2.38 (1H, s_{br}), 2.33 (2H, s_{br}), 1.79 (2H, m), 1.04 (3H, m).

2.2.3 3,3,3-(3-(3-Trifluropropylthio-1,2,5-thiadiazol-4-yl)-1,2,5,6-tetrahydro-1-methylpyridine (8)—To a stirred solution of **7** (0.98 g, 4.56 mmol) in absolute ethanol (8 ml) was added Li_2S (0.209 g, 4.56 mmol) and the mixture heated at reflux for 2 h. The mixture was cooled to rt, filtered and oxalic acid (0.451 g, 5.01 mmol) added to the filtrate. The oxalate, which precipitated out of solution, was collected by filtration and taken to the next step without further purification.

To a mixture of the oxalate in ethanol (8 ml) was added K_2CO_3 (1.57 g, 11.36 mmol) then 3-bromo-1,1,1-trifluoropropane (0.49 ml, 4.60 mmol) and the mixture heated at reflux for 1h. The mixture was cooled to rt, filtered and the filtrate concentrated. The residue purified by column chromatography on silica gel hexane/EtOAc (60/40) as the eluent. Compound **8** was obtained as a brown oil (0.458 g, 32%): ^{1}H NMR ($CDCl_3$) δ: 6.62 (1H, m), 3.34 (4H, m), 2.60 (4H, m), 2.43 (2H, m), 2.40 (3H, s). ^{13}C NMR ($CDCl_3$) δ: 156.75, 154.31, [129.77, 129.73], 127.49, 124.73, 55.60, 51.12, 45.80, [34.53, 34.25, 33.96, 33.67], 26.60, [25.11, 25.07].

2.2.4 3,3,3-(3-(3-trifluoropropylthio)-1,2,5-thiadiazol-4-yl)-1,2,5,6-tetrahydro pyridine (9)—To a solution of **8** (0.45 g, 1.46 mmol) in DCE (5 ml) was added vinyl chloroformate (0.20 ml, 2.19 mmol) and the resulting mixture heated under reflux for 2 h. After heating at reflux for 2 h the mixture was cooled to rt, water (6 ml) and conc. HCl (2 ml) were added and the mixture extracted with Et_2O (4 × 20 ml). The combined ether extract was concentrated then heated under reflux with methanolic HCl for 2 h. The solvent was then evaporated and the residue crystallized from MeOH/Et_2O to give the HCl salt of **9**. Compound **9** was obtained as the free base (brown oil, 0.206 g) by an aqueous sodium carbonate wash. HPLC analysis race contamination by **8** and the product was further

purified by column chromatography on silica gel using gradient elution: hexane to hexane/EtOAc (50/50) as the eluent. Compound **9** was obtained as a brown oil (0.252 g, 59%): ^{1}H NMR ($CDCl_3$) δ: 6.64 (1H, m), 3.76 (2H, m), 3.36 (2H, m), 2.98 (2H, m), 2.80 (1H, s_{br}), 2.58 (2H, m), 2.30 (2H, m). ^{13}C NMR ($CDCl_3$) δ: 156.89, 154.16, [133.13, 130.46], 127.45, 124.69, 46.17, 42.10, [34.47, 34.18, 33.90, 33.61], 25.79, [25.10, 25.06, 25.03, 25.00].

2.3 Radiosynthesis

The preparation of radiotracers **3**, **6** and **10** was accomplished by N-alkylation of the corresponding desmethyl precursors **2**, **5** and **9** with $^{11}CH_3I$. Though we used [^{11}C]methyl iodide and achieved sufficient yield for baboon studies without optimization, it may be possible to decrease reaction time and increase specific activity by using [^{11}C]methyl triflate [22]. Typically the following procedure was used: A solution of 1 mg precursor in DMF/DMSO (3/1), (0.25 ml) was added to a 3-necked glass vessel and the mixture cooled in a dryice/acetonitrile bath 5 mins before the release of $^{11}CH_3I$ from the GE PET trace MeI Microlab. $^{11}CH_3I$ was bubbled through the reaction mixture until maximum radioactiviy was trapped as indicated by a NaI detector. The vessel was sealed and heated in an oil bath at 100 °C for 5 mins. The vessel was then cooled by briefly dipping in a dry-ice/acetonitrile bath and HPLC eluent (1 ml) added. The resulting mixture was then purified on a Gemini semipreparative column with eluents methanol/0.025 M-pH 7.2 phosphate buffer 65/35, 70/30 and 75/25 at flow rates 5.0, 4.5 and 5.0 ml/min for **3**, **6** and **10** respectively. Elution times were 26–31, 22–27 and 28–32 min for **3**, **6** and **10** respectively. The fraction containing the labeled tracer was collected, solvent removed on a rotary evaporator, the residue redissolved in saline (4 ml) and the solution filtered through an Acrodisc syringe filter (0.2 μm, supor membrane) and collected in a sterile vial for baboon study. The entire procedure required 45–50 mins after delivery of $^{11}CH_3I$ to the reaction vessel. Specific activities, decay corrected back to end of beam (EOB) and recorded in mCi/nmol and GBq/nmol, were determined from the tracer activity obtained from Capintec readings and the mass of tracer (determined by the UV absorbance of the radiotracer and the use of calibration curves of unlabeled reference compounds).

2.4 Quality Control

The radiochemical purities were assessed by radio-TLC and radio-HPLC. For analysis of radioactive samples by radio-TLC, MN plates were developed using EtOAc/MeOH/Et_3N (80/19.8/0.2) and scanned to give R_f's of 0.60, 0.58 and 0.57 for **3**, **6** and **10** respectively, which coincided with the unlabeled standard compounds. For radio-HPLC, coelution of the respective unlabeled reference compounds with the radioactive products was used to confirm the identities of radiotracers **3**, **6** and **10**.

2.5 Log D measurement

Measurement of partition coefficients for radiotracers **3**, **6** and **10** were performed using a modified literature procedure [23]. Here, approximately 50 μl of the ^{11}C tracer solution was added to a test-tube containing octanol (2.5 ml) and a phosphate buffer solution (2.5 ml, pH 7.4) and the mixture vortexed for 2 mins then centrifuged for 2 mins. For radioactive measurements 0.1 ml of the organic layer and 1ml of the aqueous layer were placed in separate vials. Another 2 ml of the organic layer was transferred to a second test-tube containing octanol (0.5 ml) and a phosphate buffer solution (2.5 ml, pH7.4) and the procedure repeated 5 more times to give six organic sample vials and six aqueous sample vials for measuring radioactivity. Radioactivity in each vial was counted in a gamma counter and log D values calculated according to the following equation: Log D =log [(counts in octanol phase decay corrected ×10) / (counts in aqueous phase decay corrected)]

2.6 Plasma Protein Binding (PPB)

A determination of the portion of tracer in the plasma which is not bound to plasma proteins was made using the following procedure: Radioactivity in an aliquot of radiotracer was measured, added to baboon plasma (500 μl) and the mixture incubated at room temperature for 10 mins. Three 30 μl samples of the incubated mixture (bound + unbound tracer) were transferred into vials for measuring radioactivity. A 200 μl aliquot of the incubated mixture was placed in the upper level of a Centrifree tube and centrifuged for 10 min using a relative centrifugal force of ~ 2000 *g*. Three 20 μl samples of the liquid at the bottom of the Centrifree tube (the portion that contains the unbound tracer) were transferred into vials for measuring radioactivity. The portion of unbound radiotracer was calculated according to the following equation: % unbound = [(counts $_{\text{unbound}}$) / (counts $_{\text{bound + unbound}}$)] ×100.

2.7 Affinity Measurments

Affinity measurements for **3**, **6** and **10** were generously provided by the National Institute of Mental Health's Psychoactive Drug Screening Program, Contract # NO1MH32004 (NIMH PDSP). The NIMH PDSP is directed by Bryan L Roth at the University of North Carolina at Chapel Hill and Project Officer Jamie Driscol at NIMH, Bethesda MD, USA. Assays were done in duplicates using [^{3}H]quinuclidinylbenzilate (QNB), buffer mixtures, reference ligands, membranes and unlabeled test compounds **3**, **6** and **10** were used to determine equilibrium affinity constants (Ki) according to procedures described on the NIMH PDSP website: http:/pdsp.med.unc.edu.

2.8 Mouse Study

Mice were anesthetized using ketamine/xylazine (90/10, 100 mg/kg), injected intravenously with radiotracer into a tail vein and sacrificed 20 min later. Blood and brain were removed, weighed and counted to determine total activity. The blood was the centrifuged, the serum extracted with methanol (0.5 ml) and the methanol extract analysed by HPLC. The brain was placed in an equal volume of methanol and homogenized. Following centrifugation, the supernatant was analysed by HPLC. Blood and brain HPLC analyses were performed on a Spherex 5 C18 column with eluents methanol/0.01 ammonium formate buffer 85/15 at 1.0 ml/min using UV (254) and radio-detection. The unmetabolized fraction was determined by coelution with unlabeled standard compounds. One study was done for each radiotracer.

2.9 PET Study

All animal studies approved by the Brookhaven Animal Care and Use Committee. Adult female baboons were anesthetized with an intramuscular injection of ketamine hydrochloride (10 mg/kg), intubated and transported to the PET facility. Animals were maintained on a gaseous mixture of oxygen, nitrous oxide and isofluorane throughout the imaging session. Catheters were placed in an antecubital vein for radiotracer injection and in the radial artery for blood sampling. Blood pressure, respiration and heart rate were monitored throughout the imaging session. For brain imaging, the head of the baboon was positioned at the center of the field of view as defined by imbedded laser lines. For torso studies, the baboon was positioned such that the lung, heart, kidney and liver were in the view of the tomograph to be dynamically scanned at the same time. Scanning was performed for 90 mins on a high resolution PET scanner (Siemens HR+, 63 slices, 4.5×4.5×4.8 mm) in 3D mode. A transmission scan was obtained with a ^{68}Ge rotating source for attenuation correction of the emission data. Emission data were collected were collected for each tracer in 3D mode for 90 min using a 35 frame acquisition sequence for brain studies (one 10 sec; twelve 5 sec; one 20 sec; one 30 sec; eight 1 min; four 5 min; and eight 7.5 min frames) and a 22 frame sequence for torso studies (ten 1 min; four 5 min; and eight 7.5 min frames).

Generally, on a given scanning day, studies were performed in pairs: two tracer doses were administered iv, 2hrs apart to either test the reproducibility of measurements or to examine the effect of coinjecting pharmacological doses of blocking agents. Unlabeled FP-TZTP (0.025 mg/kg) and P-TZTP (0.02 mg/kg) were used as blocking agents.

2.10 Plasma Analysis

Determination of the % of unmetabolized radiotracer in the baboon's plasma was made according to literature procedures using a robot solid phase extraction (SPE) method and validated using manual HPLC analyses [24]. Robot SPE method: Radioactive measurements of baboon plasma (≈0.2 ml), sampled at various time point during the PET study were made and the plasma added to water (3 ml) at room temperature. The mixture was then applied onto Varian BondElut C18 cartridges (500 mg, preconditioned with 5 ml methanol followed 5 ml pH 7.4 phosphate buffer then preloaded with 2 ml of deionized water). Metabolite fractions were removed by a series of solvent rinses (two 5 ml deionized water rinses and two 5 ml rinses with 60% methanol in water). The radioactivity remaining on the cartridge was measured as the % of unmetabolized radiotracer. Baboon plasma sample at time zero was mixed with radiotracer and applied onto a cartridge, followed by similar solvent rinses, was used to confirm that unmetabolized radiotracer stuck to the cartridge. For validation by HPLC, baboon plasma (≈0.2 ml) sampled at various time point during the PET study was counted, added to a solution of unlabeled standard (20 μl of a 1 mg/ml solution) in methanol (1 ml) and the mixture vortexed and clarified by centrifugation. The supernatant was analyzed by HPLC (spherex 5 C18 column with eluents methanol/0.01 ammonium formate buffer 85/15 at 1.0 ml/min) using UV (254) and radio-detection. The fraction of radioactivity coeluting with the unlabeled standard, relative to the total radioactivity from the HPLC column was measured as the % of unmetabolized radiotracer. Generally recoveries from the column ranged 92–102% of the radioactivity applied to the column.

The total radioactivity in plasma for each subject for each scan was corrected for the presence of labeled metabolites, as determined by the SPE method, to obtain an input function that was used for distribution volume (DV) estimation.

2.11 Image and Data Analysis

The emission data from the dynamic scans were corrected for attenuation and reconstructed using filtered back projections. For ROI selection on the baboon brain, all time frames from dynamic images taken over the 90 min scan period were summed and planes were summed in groups of two. ROIs (striatum, cerebellum, thalamus, cortical regions etc) were drawn on the summed images then projected to the dynamic images to obtain time activity curves (TACs) expressed as %injected dose/cc (decay corrected) versus time. For the baboon torso, all time frames from dynamic images taken over the 90 min scan period were summed, ROIs drawn on the summed transaxial images and projected to dynamic images to obtain time activity curves (TACs). Distribution volumes and K_1 for brain ROIs were calculated from time-activity curves and the plasma-corrected input function using Logan plots [25]. Using TAC's, peak uptake time, clearance1/2 time and plasma integrals were compared for each tracer. Statistical analyses were done using the unpaired t test to derive two tailed p values ($p < 0.05$) to determine the statistical difference between groups of data.

3 Results and Discussion

3.1 Precursor and Radiosynthesis

Precursor compounds for radiolabeling were prepared by demethylation of unlabeled standard compounds resulting in trace contamination of the precursor by the product even after rigorous purification by column chromatography. All ^{11}C radiotracers were prepared in

high radiochemical yields. Decay corrected yields (EOB) were 74.5 ± 10.5% (n = 12), 84.5 ± 12.5% (n = 6) and 86.0 ± 2.0% (n = 10) for radiotracers **3**, **6** and **10** respectively, based on total ^{11}C activity eluting the chromatography column. Radiochemical purity was greater than 99% for all radiotracers synthesized. Specific activities at EOB, 14.5 ± 8.6 mCi/nmol (0.54 ± 0.32 GBq/nmol, n = 12), 9.3 ± 5.1 mCi/nmol (0.34 ± 0.19 GBq/nmol, n = 6) and 8.0 ± 4.0 mCi/nmol (0.30 ± 0.15 GBq/nmol, n = 10) for radiotracers **3**, **6** and **10** respectively, were comparable to other ^{11}C tracers prepared at our laboratory, despite the potential for lowering of specific activities by trace contamination of the precursors by the corresponding unlabeled products. Mass at time of injection was 1.32 ± 0.85 μg (0.088 ± 0.056 μg/kg, n = 12), 1.47 ± 0.75 μg (0.098 ± 0.050 μg/kg, n = 6) and 1.86 ± 0.92 μg (0.124 ± 0.061 μg/kg, n = 10) for radiotracers **3**, **6** and **10** respectively. No reports are available in the literature for concentrations of M2 receptors in the baboon brain while pmol/mg concentrations (0.21–2.51 pmol/mg) are reported for the rat brain [26] and fmol/mg concentrations (mean, 15–65 fmol/mg) are reported for the human brain [27]. Estimates of the percentage occupancy by radiotracers **3**, **6** and **10**, in baboon striatum, visual cortex and temporal cortex were made using the respective molecular weights, mean injected masses, maximum percent ID/g in tissue, in vitro affinity constants as determined by NIMH PDSP, and receptor concentration in human brain [26] as no B_{max} values are available for the baboon brain in the literature. For radiotracer **3** receptor occupancy was estimated to be 3%, 2% and 2% respectively for the baboon striatum, visual cortex and temporal cortex. For radiotracer **6** receptor occupancy was estimated to be 4%, 3% and 3% respectively for the baboon striatum, visual cortex and temporal cortex while for radiotracer **10** receptor occupancy was estimated to be 2% each for the same brain regions. The low receptor occupancies (2–4%) in these studies would not be expected to violate the tracer principle. For each of the radiotracers in this study, there were no significant correlations between the injected mass and the DV's.

3.2 Log D and PPB

Log D values, 2.4 ± 0.1 (n=5), 2.9 ± 0.2 (n=2) and 2.9 ± 0.03 (n=2) for **3**, **6** and **10** respectively, were all in the optimal range (1–3) for blood brain barrier (BBB) penetration. Plasma free fractions were 8.0 ± 0.9% (n=6), 3.9 ± 0.1% (n=4) and 4.1 ± 1.0% (n=4) for **3**, **6** and **10** respectively compared to the free fraction of [^{18}F]FP-TZTP, radiotracer **3** labeled with F-18, reported previously (10.4 ± 2.0%) [11].

3.3 Affinity Constants

To assess the relative M2 affinities of compounds **3**, **6** and **10** in vivo, in vitro affinity measurements were made (results shown in Table 1).

Affinity constants differ from those in the literature [12] possibly due to the different assay conditions used in this study. The data suggests that, for each compound, there is little or no difference in the affinities for the receptor subtypes studied and little difference in the affinity of each compound for the M2 receptor. These results do not support studies that shows clear M2 selectivity for [^{18}F]FP-TZTP in vivo in KO mice studies [13–14]. Our findings of little or no in vitro subtype selectivity is not an isolated observation, in fact Ravasi and coworker also found no in vitro subtype selectivity for [^{18}F]FP-TZTP using Chinese hamster ovarian cells expressing the five subtypes of human muscarinic receptors [28]. Using in vitro off-rate studies, they showed that the slower dissociation kinetics of FP-TZTP from M2 receptors compared with the other muscarinic receptor subtypes may contribute to its M2 selectivity. These results show for muscarinic receptors in vitro affinity constants are not sufficient to predict in vivo pharmacokinetics.

3.4 Mouse data

To assess the possibility that labeled metabolites of **3**, **6** and **10** could be present in the baboon brain during the time course of the PET studies, analysis of the brain and blood in mice, 20 min after radiotracer injection, were made (results shown in Table 2).

Similar to the baboon plasma data (Table 3) the fraction of ^{11}C present as labeled metabolites is lower for **10** as compared to **3**. However, unlike that for the baboon the fraction of ^{11}C present as labeled metabolites in the mouse plasma is lower for **6** as compared to **3**.

The rate of peripheral metabolism for [^{18}F]FP-TZTP has been reported to be much faster in rats as compared to primates (factor of 2.5) [9], and for this reason we expect that parent radiotracers (**3**, **6** and **10**) will predominate in the baboon brain during the time course of the PET studies.

3.5 Baboon Plasma Analysis

For each radiotracer the total C-11 concentration vs time and the fraction of radiotracer present as parent at selected times was measured (Table 3). This information was used to obtain a plasma input function corrected for the presence of labeled metabolites. We note that there is considerable inter-animal variability as is evident from the large standard deviations and that prior studies with [^{18}F]FP-TZTP in rhesus monkeys report similar percentages of parent radiotracer in plasma as compared to the ^{11}C-fluoropropylthio and propylthio-TZTP derivatives in this study [9].

Using the unpaired t-test to analyze the data summarized in Table 3 we find that the fluoropropyl and propyl derivatives have similar metabolic rates while the trifluoropropyl derivative is metabolized at a significantly slower rate ($p < 0.05$) after 10 min. A prior LC-MS study of the profile of metabolites from [^{18}F]FP-TZTP in rat and human hepatocytes reported that the N-oxide compound produced by oxidation of the nitrogen atom in the 1-methyltetrahydropyridine ring (which does not cross the blood brain barrier) is the major metabolite [29]. The other metabolites arise from sulfur oxidation, demethylation of the tertiary amine (which would not be labeled) and oxidation of the tetrahydropyridine ring. Monkeys have been reported to have a similar metabolic profile with different proportions of the metabolites [9]. In addition to the above mentioned metabolites oxidation of the alkyl side chain to give a terminal acid is possible for compound **6**, whereas the fluorine atoms of compounds **3** and **10** should inhibit such side chain oxidation. Such alkyl side chain oxidation metabolites have been reported for related compounds [30–32]. For the TZTP derivatives under study, most of the major metabolites would be more polar than the parent compounds and would be predicted to have lower blood brain barrier penetration.

The time course for tracers **3**, **6** and **10** (both total C-11 and for C-11 as parent radiotracer) in the baboon plasma during the PET study, in the same animal is shown in Figure 3.

Averaged AUC data (expressed as the area under the metabolite corrected time-activity curve) is shown in Table 4. Here a major difference can be seen for the fluoropropyl and the propyl derivatives on one hand and the trifluoropropyl derivative on the other hand with the AUC for the trifluoropropyl derivative being 2–3 fold smaller than for the fluoropropyl and propyl derivatives. The difference is apparent at early and late times and is likely due to the higher retention of **10** in peripheral organs.

3.6 Kinetic Analysis

3.6.1 In vivo Kinetics and Biodistribution in Baboon Brain—The magnitude and rate of brain uptake and clearance differed for **3**, **6** and **10** with **10** showing significantly lower and slower uptake and clearance than **3** and **6**, in the same animal. This is shown in figure 4.

In general, for **3**, tissue uptake was rapid followed by rapid clearance, similar to the ^{18}F analogue reported previously which is expected if there is no significant entry of labeled metabolites into the brain [9,11]. The highest uptake was observed in the striatum with the cerebellum peaking earliest and clearing fastest for **3**. For **6**, the highest uptake also occurred in the striatum but clearance was slower. For **10**, C-11 uptake was highest in the cerebellum but clearance was slower in all brain regions as compared to **3** and **6**. In addition, kinetics was similar for different brain regions for **10**.

3.6.2 Baseline comparison of 3, 6 and 10—From the TACs in the different brain regions and the plasma input functions we have estimated K_1 (plasma to brain transfer constant) and distribution volumes (DV) for **3**, **6** and **10**. These are shown in Table 5 with comparative values from the literature for [^{18}F]FP-TZTP in the rhesus monkey [11]. Radiotracer uptake in the brain is rapid for each radiotracer as evidenced by K_1 values which ranged from 0.6 to 1.5 ml/min^{-1}/ml^{-1}.

We note that the DV values for [^{11}C]FP-TZTP and [^{18}F]FP-TZTP are remarkably similar to each other and to [^{11}C]P-TZTP for most brain regions. For tracer **3** most of the labeled metabolites are identical to those of the ^{18}F-tracer while for tracer **6** the labeled metabolites may be different where oxidation of the alkyl side chain is also possible. DV values for **3** and **6** are similar to the ^{18}F-tracer even though different approaches were used to derive the values. Carson et al [11] derived DV values for the rhesus monkey using a one compartment model while DV values in this study were derived for the baboon from graphical analysis using Logan plots [25]. The addition of two more fluorine atoms in **10** results in significantly different kinetics as compared to **3** and **6**. This is reflected in a much slower loss from tissue most likely due to a decrease in the receptor ligand dissociation constant (k_{off}). This results in a much higher DV. The slow kinetics makes it difficult to accurately estimate the DV resulting in an apparent loss of dynamic range in the regional DV values.

Prior studies with [^{18}F]FP-TZTP in rhesus monkeys, reported similar values for DV's (22–26 ml/ml) in cortical regions, thalamus and basal ganglia and significantly lower values in the cerebellum [11], in contrast to humans where the cerebellum and basal ganglia had the highest DVs while the thalamus and occipital cortex had the lowest DVs [15].

We note that the kinetics of each tracer is reproducible as observed in the cerebellum and striatum in test-retest studies in the same animal; variability in the DV's for test-retest is ~10% for **3** and **6** and ~25% for **10** (data not shown).

Co-injection of unlabeled FP-TZTP (90 nmol/kg) with **3**, **6** and **10** resulted in reduced uptake for each labeled compound, with **10** showing the greatest reduction (see Figure 5 for T-A curves for the striatum and cerebellum at baseline and after FP-TZTP treatment for **3**, **6** and **10**). The % reduction in DV by coinjection with unlabeled FP-TZTP is given in Table 6. Unlabeled P-TZTP was also effective at inhibiting uptake of **3**, **6** and **10** in coinjection studies (data not shown).

Inhibition of uptake by FP-TZTP (or P-TZTP) is greatest for **10**. We note that Kiesewetter *et al.* [11], also report robust (>50%) reductions in DVs of approximately in the monkey brain, by preadministering 200 to 400 nmol/kg of nonradioactive FP-TZTP. The inhibitions of

[^{18}F]FP-TZTP binding by FP-TZTP or P-TZTP were also reported to be essentially identical in rats [33]. The lower doses used in these studies may account for the observed difference in degrees of blockade for FP-TZTP and P-TZTP.

3.7 Comparison of Uptake and kinetics of 3, 6 and 10 in Peripheral Organs

Time activity curves for radiotracers **3**, **6** and **10** in peripheral organs are shown in Figure 6. Comparable rates of uptake and clearance were observed for **3**, **6** and **10** in the kidney and lung. The heart has a large concentration of M2 receptors. The highest uptake in the heart was observed for **3**, while **10** cleared the slowest. The uptake of **10** in the liver was almost twice as high as compared to **3** and three times as high as compared to **6**. This much more rapid removal of **10** and/or its labeled metabolites from the blood by the liver may contribute to the lower concentration of **10** in the plasma (Table 4).

4 Conclusion

Labeling FP-TZTP with carbon-11 produces a radiotracer with similar brain kinetics and binding properties in the baboon to the ^{18}F-labeled molecule reported previously [10]. This indicates that [^{11}C]FP-TZTP will be suitable for translation in humans for serial studies or for pairing with other radiotracers in the same day. In addition, making small structural variations on the side chain of FP-TZTP only slightly changed brain kinetics in the case where fluoropropylthio was changed to propylthio-TZTP. However, changing fluoropropyl to trifluoropropyl drastically changed the kinetics in both brain and peripheral organs while only minimally affecting log D and plasma protein binding. For the TZTP derivatives studied in vitro affinities for M2 receptors do not predict in vivo pharmacokinetics. Though all three tracers showed binding to M2 receptors as evidenced by blockade with unlabeled FP-TZTP and P-TZTP, the trifluoropropyl derivative showed the largest degree of blockade. However the slow kinetics of the tracer led to difficulties in accurately estimating the DVs and % changes. As a result there was no discernable difference in DV between the different brain regions. Also the increased retention in peripheral organs contributed to the smaller plasma input for **10**. This leads to lower brain uptake for a given dose contributing to an increase in noise with radioactive decay. Additionally the increased retention results in a greater whole body radiation dose. In radiotracer development, an examination of peripheral organ kinetics is useful for getting a broad perspective on factors governing brain kinetics.

This study highlights the difficulty of predicting the in vivo behavior of radiopharmaceuticals even when requirements of log D, molecular weight and PPB, commonly used screening tools, are met. Though in vitro affinities generally predict suitable candidates for in vivo studies, in the case of muscarinic receptors such data fails to give leads. Insufficient tools to differentiate among potential radioligands ex vivo, continues to be a limiting factor in radiotracer development.

Acknowledgments

This work was supported by the US Department of Energy's Office of Biological and Environmental Research and by NIH (K05-DA020001). The authors wish to thank Dr. Bryan Roth, Mr. Jon Evans and the NIMH Psychoactive Drug Screening Program for conducting the binding assays of the TZTP derivatives. Sincere thanks also to Michael Schueller, Lisa Muench, Pauline Carter, Payton King and Donald Warner of the PET Imaging Group at Brookhaven National Laboratory.

References

1. Aubert I, Araujo DM, Cecyre D, Robitaille Y, Gauthier S, Quirion R. Comparative alterations of nicotinic and muscarinic binding sites in Alzheimer's and Parkinson's diseases. Journal of Neurochemistry. 1992a; 58:529–541. [PubMed: 1729398]

2. Rodriguez-Puertas R, Pascual J, Vilaro T, Pazos A. Autoradiographic distribution of M1, M2, M3 and M4 muscarinic receptor subtypes in Alzheimer's disease. Synapse. 1997; 26:341–350. [PubMed: 9215593]
3. Quirion R, Aubert I, Labchak PA, Schaum RP, Teolis S, Gauthier S, Araujo DM. Muscarinic receptor subypes in human neurodegenerative disorders; focus on Alzheimer's disease. Trends in Pharmacologic Science. 1989:80–84.
4. Li M, Yasuda RP, Wall SJ, Wellstein A, Wolfe BB. Distribution of m2 muscarinic receptors in rat brain using antisera selective for M2 receptors. Mol Pharmacol. 1991; 40:28–35. [PubMed: 1857338]
5. Flyn DD, Mash DC. Distinct kinetic binding properties of N-[3H]-methylscopolamine afford differential labeling and localization of M1, M2 and M3 muscarinic receptor subtypes in primate brain. Synapse. 1993; 14:283–296. [PubMed: 8248852]
6. Lipinski CA. Lead- and drug-like compounds: the rule-of-five revolution. Drug Discov Today Technol. 2004; 1:337–341.
7. Sauerberg P, Olesen PH, Nielsen S, Treppendahl S, Sheardown MJ, Honoré T, Mitch CH, Ward JS, Pike AJ, Bymaster FP, Sawyer BD, Shannon HE. Novel functional M_1 selective muscarinic agonists. Synthesis structure-activity relationships of 3-(1,2,5-thiadiazoyl)-1,2,5,6-tetrahydro-1-methylpyridines. J Med Chem. 1992; 35:2274–2283. [PubMed: 1613751]
8. Knol R, Doornbos T, Bos J, Bruin K, Pfaffendorf M, Aanhaanen W, Janssen AG, Vekemans JA, van Eck-Smit BL, Booij J. Synthesis and evaluation of iodinated TZTP-derivatives as potential radioligands for imaging of muscarinic M2 receptors with SPET. Nucl Med Biol. 2004; 31:111–123. [PubMed: 14741576]
9. Kiesewetter DO, Carson RE, Jagoda EM, Herscovitch P, Eckelman WC. In vivo muscarinic binding of 3-(alkylthio)-3-thiadiazoyl tetrahydropyridines. Synapse. 1999; 31:29–40. [PubMed: 10025681]
10. Farde L, Suhara T, Halldin C, Nyback H, Nakashima Y, et al. PET study of the M1-agonist [^{11}C]xanomeline and [^{11}C]butylthio-TZTP in monkey and man. Dementia. 1996; 7:187–195. [PubMed: 8835881]
11. Carson RE, Kiesewetter DO, Jagoda EM, Der MG, Herscovitch P, Eckelman WC. Muscarinic cholinergic receptor measurements with [^{18}F]FP-TZTP: control and competition studies. J Cereb Blood Flow Metab. 1998; 18:1130–1142. [PubMed: 9778190]
12. Kiesewetter DO, Lee J, Lang L, Park SG, Paik CH, Eckelman WC. Preparation of ^{18}F-labeled muscarinic agonist with M2 selectivity. J Med Chem. 1995; 38:5–8. [PubMed: 7837240]
13. Jagoda EM, Kiesewetter DO, Shimoji K, Yamada M, Gomeza J, Wess J, Eckelman WC. Regional brain uptake of the muscarinic ligand [^{18}F]FP-TZTP, is greatly decreased in M2 receptor knockout mice but not in M1, M3 and M4 receptor knockout mice. Neuropharmacology. 2003; 44:653–661. [PubMed: 12668051]
14. Eckelman WC. The use of gene-manipulated mice in the validation of receptor binding radiotracer. Nucl Med Biol. 2003; 30:851–860. [PubMed: 14698789]
15. Podruchny TA, Connolly C, Bokde A, Herscovitch P, Eckelman WC, Kiesewetter DO, Sunderland T, Carson RE, Cohen RM. In vivo muscarinic 2 receptor imaging in cognitively normal young and older volunteers. Synapse. 2003; 48:39–44. [PubMed: 12557271]
16. Cohen RM, Podruchny TA, Bokde A, Carson RE, Herscovitch P, Kiesewetter DO, Eckelman WC, Sunderland T. Higher in vivo muscarinic-2 receptor distribution volumes in aging subjects with an Apolipoprotein E-epsilon4 allele. Synapse. 2003; 48(9):150–156. [PubMed: 12774299]
17. Cannon DM, Carson RE, Nugent AC, Eckelman WC, Kiesewetter DO, et al. Reduced muscarinic type 2 receptor binding in subjects with Bipolar disorder. Arch Gen Psychiatry. 2006; 63:741–747. [PubMed: 16818863]
18. Benson BE, Carson RE, Kiesewetter DO, Herscovitch P, Eckelman WC, Post RM, Ketter TA. A potential cholinergic mechanism of procaine's limbic activation. Neuropsychopharmacology. 2004; 29:1239–1250. [PubMed: 14997171]
19. Perrin, DD.; Armarego, WL. Purification of Laboratory Chemicals. 3rd ed.. New York: Pergamon Press Inc; 1988.
20. Bell TW, Choi HJ, Harte W, Drew MG. Synthesis, conformatios and basicities of bicyclic triamines. J Am Chem Soc. 2003; 125:12196–12210. [PubMed: 14519005]

21. Yu KH, Park JH, Yang SD. Synthesis of [^{18}F]fluorocholine analogues as a potential imaging agent for PET studies. Bull Korean Chem Soc. 2004; 25(4):506–510.
22. Någren K, Müller L, Halldin C, Swahn C, Lehikonen P. Improved synthesis of some commonly used PET radioligands by the use of [^{11}C]methyl triflate. Nucl Med Biol. 1995; 22:235–239. [PubMed: 7767319]
23. Wilson AA, Jin L, Garcia A, DaSilvain JN, Houle S. An admonition when measuring the lipophilicity of radiotracers using counting techniques. Appl Radiat Isot. 2001; 54:203–208. [PubMed: 11200881]
24. Ding YS, Lin KS, Garza V, Carter P, Alexoff D, Logan J, Shea C, Xu Y, King P. Evaluation of a new norepinephrine transporter PET ligand in baboons, both in brain and peripheral organs. Synapse. 2003; 50:345–352. [PubMed: 14556239]
25. Logan J. Graphical analysis of PET data applied to reversible and irreversible tracers. Nucl Med Biol. 2000; 27:661–670. [PubMed: 11091109]
26. Li M, Yasuda R, Wall S, Wellstein A, Wolfe B. Distribution of m2 muscarinic receptors in rat brain using antisera selective for m2 receptors. Mol. Pharmacol. 1991; 40:28–35. [PubMed: 1857338]
27. Rodriguez-Puertas R, Pascual J, Vilaro T, Pazos A. Autoradiographic distribution of M1, M2, and M3 and M4 muscarinic receptor subtypes in Alzheimer's disease. Synapse. 1997; 26:341–350. [PubMed: 9215593]
28. Ravasi L, Kiesewetter DO, Shimoji K, Lucignani G, Eckelman WC. Why does the agonist [^{18}F]FP-TZTP bind preferentially to the M2 muscarinic receptor? Eur J Nucl Med Mol Imaging. 2006; 33:292–300. [PubMed: 16333673]
29. Ma Y, Kiesewetter DO, Jagoda EM, Huang BX, Eckelman WC. Identification of metabolites of fluorine-18-labeled M2 muscarinic receptor agonist, 3-(3-[(3-fluoropropyl)thio]-1,2,5-thiadiazol-4-yl)-1,2,5,6-tetrahydro-1-methylpyridine, produced by human and rat hepatocytes. J Chromatography B. 2002; 766(2):319–329.
30. Gillespie TA, Lindsay TJ, Cornpropst D, Bonate PL, Skaggs TG, Delong AF, Shipley LA. Biological and biotechnological applications of ESI-MS, ACS symposium series. American Chemical society. 1996; 619:315.
31. Murphy AT, Bonate PL, Kasper SC, Gillespie TA, Delong AF. Determination of xanomeline in human plasma by ionspray tandem mass-spectrometry. Biol. Mass Spectrom. 1994; 23:621–625. [PubMed: 7986832]
32. Murphy AT, Kasper SC, Gillespie TA, Delong AF. Determination of xanomeline and active metabolite, N-desmethylxanomeline, in human plasma by liquid chromatography-atmospheric pressure chemical ionization mass spectrometry. J. Chromatogr. B. 1995; 668:273–280.
33. Shimoji K, Esaki T, Itoh Y, Ravasi L, Cook M, Jehle J, Jagoda EM, Kiesewetter DO, Schmidt K, Sokoloff L, Eckelman WC. Inhibition of [^{18}F]FP-TZTP binding by loading doses of muscarinic agonists P-TZTP or FP-TZTP in vivo is not due to agonist-induced reduction in cerebral blood flow. Synapse. 2003; 50:151–163. [PubMed: 12923818]

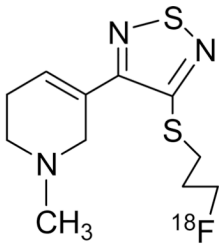

[18F] FP-TZTP

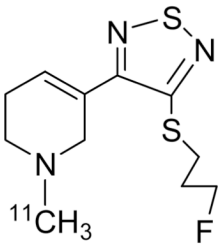

[11C] FP-TZTP, 3

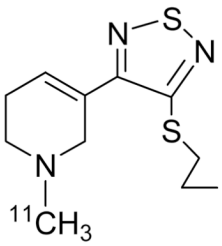

[11C] P-TZTP, 6

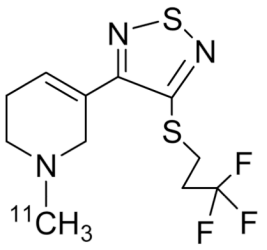

[11C] F3P-TZTP, 10

Figure 1.
Radioligands for PET imaging muscarinic M2 receptors.

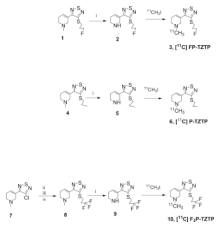

Figure 2.
Synthesis of radiotracers **3**, **6** and **10**.
Reagents. i. vinylchloroformate, DCE; ii. Li_2S, EtOH; iii. oxalic acid; iv. bromotrifluoropropane, K_2CO_3, EtOH.

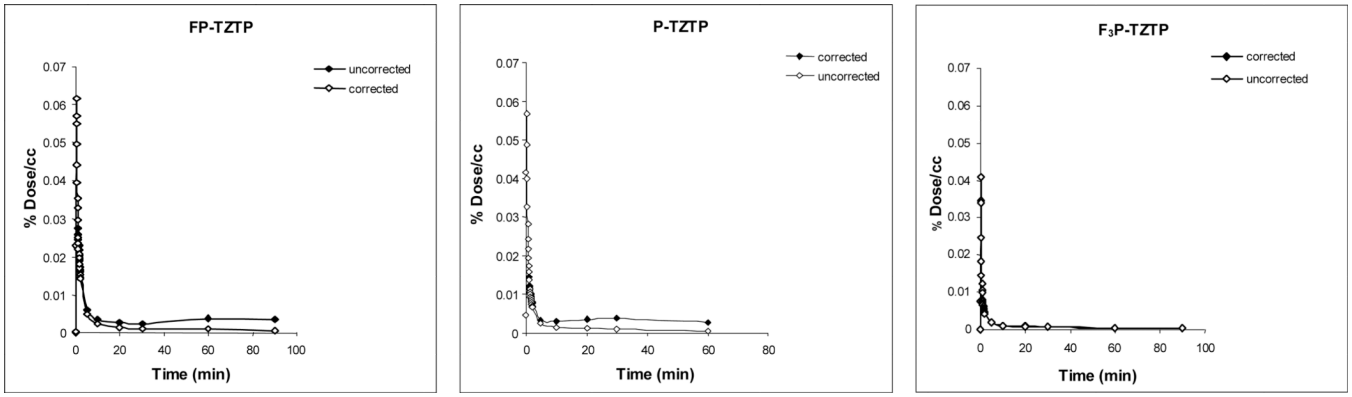

Figure 3.
Time activity curves of radioligands in baboon plasma uncorrected and corrected for labeled metabolites.

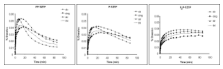

Figure 4.
Time activity curves for radiotracers in brain regions of the same baboon.

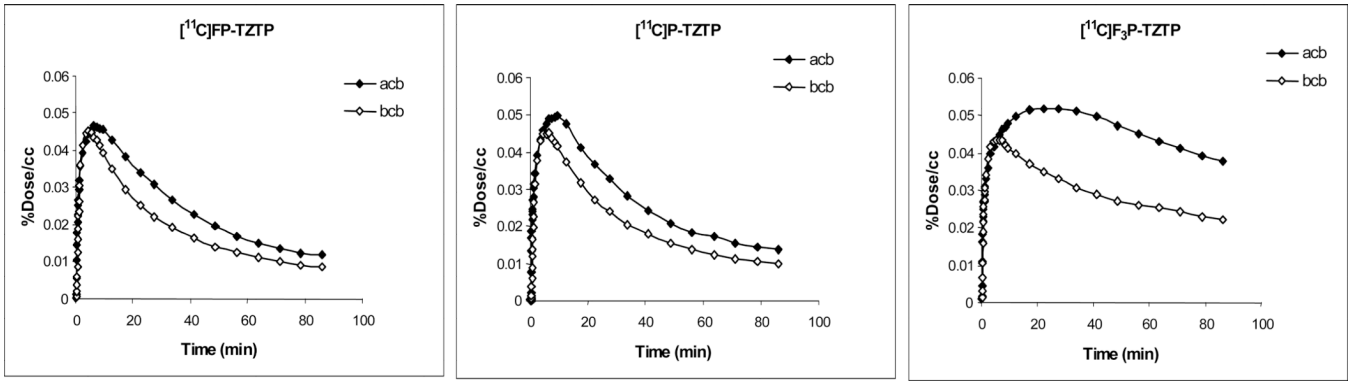

Figure 5.
Time activity curves for radiotracers in the cerebellum of the same baboon baseline and after coinjection with unlabeled FP-TZTP.

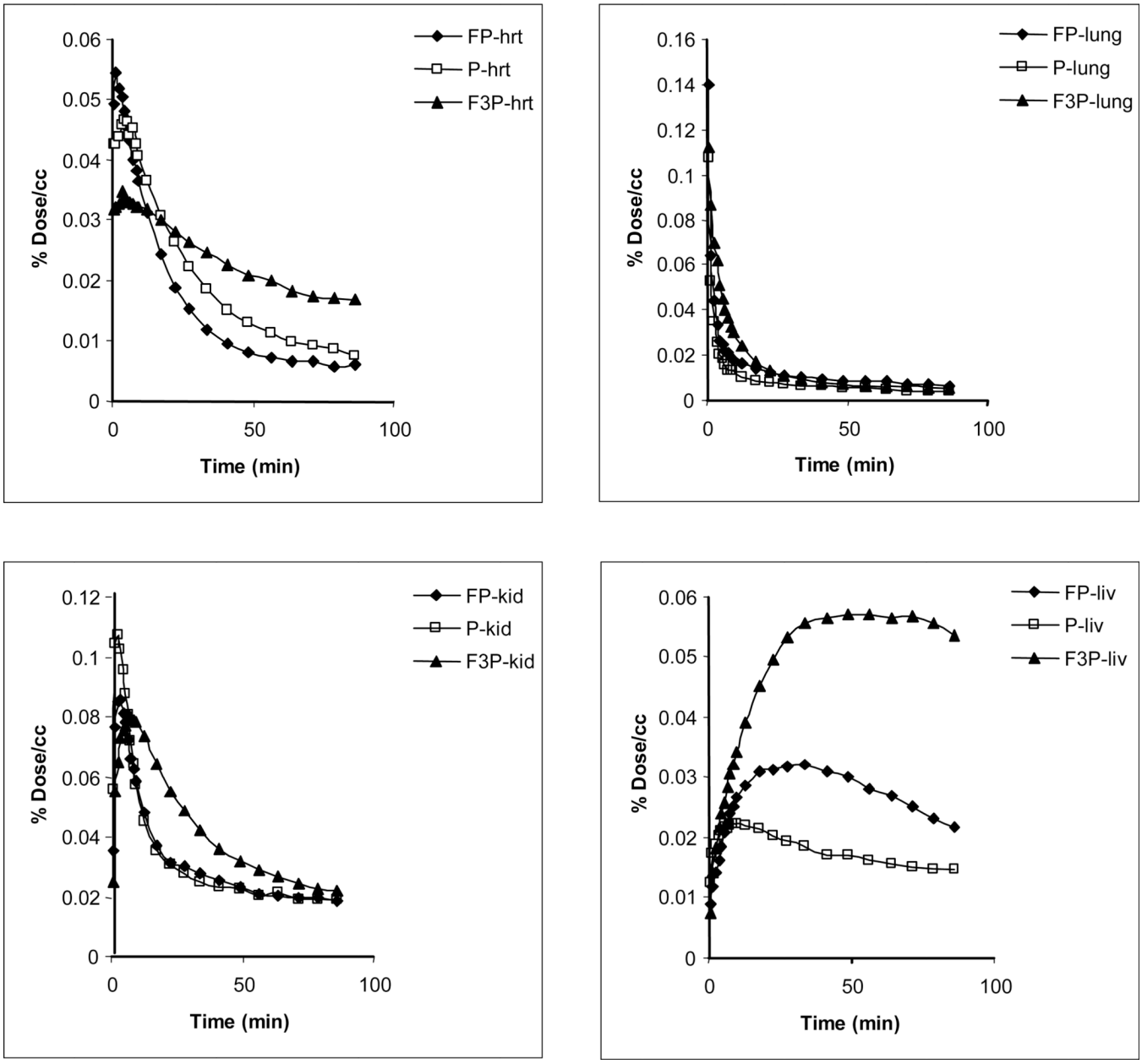

Figure 6.
Time activity curves for radiotracers in baboon peripheral organs.

Table 1

In Vitro affinity constants reported as mean ± error values as determined by the NIMH PDSP using [^{3}H]QNB (literature values in parentheses [11])*.

Compound	M1 (nM)	M2 (nM)
FP-TZTP	59.0 ± 4.6 (7.4)	38 ± 3.2 (2.2)
P-TZTP	51 ± 4.0 (23)	24 ± 1.9 (1.5)
F_3P-TZTP	119 ± 9.45	112 ± 14.9

*[^{3}H]Piperizepine was used with bovine striatal membranes for M1 and [^{3}H]AF-DX384 was used for rat heart membranes for M2 in the literature [11].

Table 2

% Parent radiotracer in mouse brain and blood.

Tracer	Brain	Blood
^{11}C-FP-TZTP (**3**)	95	5
^{11}C-P-TZTP (**6**)	93	15
^{11}C-F$_3$P-TZTP (**10**)	94	11

One mouse study was done for each radiotracer.

Table 3

Percent parent radiotracer in baboon plasma after bolus injection represented as the mean ± standard deviation.

Time (min)	[^{11}C]FP-TZTP(n=5)	[^{11}C]P-TZTP (n=5)	[^{11}C]F$_3$P-TZTP (n=5)
1	92 ± 4	91 ± 5	95 ± 2
5	84 ± 5	83 ± 4	90 ± 4
10	64 ± 14	66 ± 9	84 ± 5
30	26 ± 8	32 ± 11	61 ± 14
60	20 ± 7	21 ± 5	48 ± 18
90	13 ± 3	12 ± 3	22 ± 2

[a] There is no significant difference ($p < 0.05$) in % parent radiotracer between ^{11}C-FP-TZTP and ^{11}C-P-TZTP at any of the time points studied.

[b] For ^{11}C-F$_3$P-TZTP the % parent radiotracer is significantly lower ($p < 0.05$) than for ^{11}C-FP-TZTP and ^{11}C-P-TZTP after 10 min.

Table 4

Plasma integral corrected and uncorrected for metabolites at 60 min and 90 min.

Radiotracer	Plasma Integral Mean (±SD)			
	60 min uncorrected	60 min corrected	90 min uncorrected	90 min corrected
^{11}C-FP-TZTP (n=7)	2608 ± 196	1318 ± 212	3452 ± 274	1459 ± 245
^{11}C-P-TZTP (n=5)	2651 ± 394	1462 ± 258	3469 ± 502	1604 ± 297
^{11}C-F_3P-TZTP (n=5)	884 ± 179	695 ± 98	1095 ± 255	776 ± 106

[a] There is no significant difference ($p < 0.05$) between 60 min and 90 min metabolite corrected values for any of the three radiotracers.

[b] For ^{11}C-F_3P-TZTP there is no significant difference among uncorrected and corrected at 60 min or 90 min.

Table 5

Comparison of K_1's and DVs for **3** (n=8), **6** (n=5) and **10** (n=4) in the baboon brain using baseline studies represented as the mean ± standard deviation. Values are also shown for [^{18}F] FP-TZTP in rhesus monkey brain for comparison [10].

Tracer	cerebellum	striatum	thalamus	cingulate	parietal	occipital	temporal
K_1's							
^{11}C-FP-TZTP	1.03 ±0.37	0.97 ±0.40	0.92 ±0.56	0.68 ±0.27	0.63 ±0.29	0.92±0.36	0.66 ±0.25
^{11}C-P-TZTP	0.78 ±0.27	0.67 ±0.15	0.61 ±0.16	0.50 ±0.13	0.44 ±0.11	0.56 ±0.10	0.50 ±0.12
^{11}C-F_3P- TZTP	1.49 ±0.54	1.49 ±0.57	1.24 ±0.50	0.94 ±0.34	0.79 ±0.28	1.10 ±0.43	0.96 ±0.29
[^{18}F] FP-TZTP	0.62 ±0.27	0.52 ±0.24	0.51 ±0.23	0.48 ±0.23	0.40 ±0.21	0.38 ±0.17	0.47 ±0.20
DV's							
^{11}C-FP-TZTP	13.9 ±2.6	22.0 ±3.5	17.6 ±3.9	19.0 ±3.7	19.7 ±4.3	17.0 ±5.0	20.3 ±4.4
^{11}C-P-TZTP	17.8 ±1. 7	25.0 ±3.3	20.0 ±1.9	23.2 ±2.4	22.6 ±2. 6	20.8 ±3.1	24.3 ±3.0
^{11}C-F_3P- TZTP	139.6 ±32.7	150.0 ±55.9	174.3 ±71.1	176.6 ±65.8	160.7 ±69.8	143.1 ±56.2	175.1 ±68.0
[^{18}F] FP-TZTP	15.7 ±3.8	25.6 ±5.8	23.2 ±6.1	26.5 ±7.5	25.5 ±6.9	21.7 ±6.0	24.4 ±5.3

[a] For ^{11}C-FP-TZTP with the exception of the occipital, the cerebellum has a significantly smaller DV ($p < 0.05$) than other brain regions.

[b] For ^{11}C-P-TZTP with the exception of the occipital and thalamus, the cerebellum has a significantly smaller DV ($p < 0.05$) than other brain regions.

[c] For ^{11}C-F_3P-TZTP there is no significant difference in DV ($p < 0.05$) for all brain regions studied.

[d] With the exception of the cerebellum and the cingulate DVs for a given brain region is similar for ^{11}C-FP-TZTP and ^{11}C-P-TZTP.

[e] ^{11}C-F_3P-TZTP has significantly larger DVs ($p < 0.05$) in all brain regions as compared to ^{11}C-FP-TZTP and ^{11}C-P-TZTP.

Table 6

Percent decrease in DV with co-injection of unlabeled FP-TZTP in the same baboon.

Tracer	cerebellum	striatum	thalamus	cingulate	parietal	occipital	temporal
^{11}C-FP-TZTP	22	34	49	23	37	-	36
^{11}C-P-TZTP	25	33	31	33	32	37	35
^{11}C-F_3P-TZTP	47	52	55	55	49	47	48

One study (basline followed by coinjection 2hr apart) was done for each radiotracer.